Acoust. Sci. & Tech. **43**, 5 (2022)

PAPER

A 3D-printed sound-absorbing material based on multiple resonator-like unit cells for low and middle frequencies

Akiko Sugahara*

Faculty of Architecture, Kindai University,
3–4–1 Kowakae, Higashiosaka, 577–8502 Japan

(*Received 6 December 2021, Accepted for publication 5 June 2022*)

Abstract: Inorganic fiber-based porous materials, such as glass and rock wool, are cost-effective, light weight, and currently make up the most commonly used sound-absorbing materials. However, the performance of these materials degrades owing to moisture, weather, and gravity. Porous materials have difficulty absorbing low-frequency sounds. In these cases, resonator-type sound-absorbers are used, but the target frequency is narrow. Thus, a novel sound-absorbing material that solves these issues is desired. Recently, the advancement of additive manufacturing enabled the realization of complex structures, and artificial acoustic materials have attracted significant attention. This study conducted numerical, theoretical, and experimental investigations to develop novel sound-absorbing materials with desired sound absorption properties based on a flexible situation. These materials also address aforementioned problems in conventional inorganic porous materials and resonators. Results suggest that the periodic structures based on resonators and their combination are good sound-absorbers for low- and middle-frequency ranges, exploiting the properties of each structure.

Keywords: Absorbing material, Periodic structure, Coupling resonators, Acoustic metamaterial

1. INTRODUCTION

The mission of acoustic room design is to create a comfortable acoustic environment, and includes maintaining a quiet space by controlling environmental noise generated around the room, making music sound delightful, and clearly transmitting speech. To achieve these goals, appropriate sound-absorbing materials must be used according to the purpose of the room.

Inorganic fiber-based porous materials, such as glass and rock wool, are widely used sound-absorbing materials owing to their low cost, light weight, and high acoustic performance over a relatively wide range of frequencies. However, performance degradation due to moisture, weather, and gravity is challenging. For example, conventional inorganic porous materials lose performance stability as the fibers settle over time and as the density changes between the upper and lower parts. Similar degradation occurs when the binder deteriorates because of internal condensation, causing the fibers to sag and slide down. Further, moisture content contributes to a loss in thickness [1]. Another problem with inorganic porous materials is insufficient sound absorption performance in lower-frequency ranges. A resonator is often used in such cases, but it is difficult for a resonator-type mechanism to absorb sound over a wide frequency range without inserting an inorganic porous material behind it.

Under these circumstances, a novel sound-absorbing material is desired, that solves these problems with a high sound absorption coefficient over a broadband of low and medium frequencies without degradation.

Over the years, many researchers have worked to develop novel sound-absorbing materials, e.g., the micro-perforated panel absorber. Theoretical elucidation of its absorbing properties [2,3] and numerical and experimental analysis led to its practical application in the 1990s [4–6]. Recently, derived structures, such as the double-leaf MPP panel, honeycomb-backed MPP panel, and double-leaf panel with a permeable membrane, have been developed and investigated by experimental and numerical analysis [7,8]. Sanada and Tanaka theoretically and experimentally indicated that two resonant peaks are observed by connecting two resonators in series to form a two-degree-of-freedom system. The lower peak appears at a lower frequency than the original one-degree-of-freedom system [9,10]. This series-coupled resonator allows the sound absorption coefficient to have multiple peaks. This kind of structure is also investigated for applications such as sound trapping in ducts [11].

*e-mail: sugahara@arch.kindai.ac.jp
[doi:10.1250/ast.43.251]

In recent years, with the advancement of additive manufacturing, complex structures have been realized, which has attracted artificial materials, such as acoustic metamaterials. Additive manufacturing, or three-dimensional (3D) printing technology, makes it possible to create sound-absorbing materials with desired properties [12–14]. Furthermore, by selecting the appropriate material, these 3D printed sound-absorber structures can solve the problems of conventional porous fibers. For example, if a sound-absorber is fabricated using a rigid and robust material, fiber settling due to gravity and moisture will not occur. Thus, the structure does not deteriorate because of the shape change described above, even after a long time.

In terms of artificial structural design, some researchers [15–19] have developed porous sound-absorbing materials with micro-periodic structures based on different types of simple representative elementary units (REVs), such as the body-centered cubic. Zieliński *et al.* [17] systematically summarized this approach and reported benchmark problems. Some studies have indicated the relationship between a simple REV configuration and its macroscopic sound absorption properties via numerical analysis and experimental investigation [14,18,20]. However, only few studies report the type of structure that exhibits the desired sound absorption characteristics; thus, a design-based approach is required. In particular, studies focusing on sound absorption in the low-frequency range and studies combining multiple structures have not been conducted. The design of materials that combines multiple structures and uses their advantage will lead to the development of sound-absorbing materials with great flexibility.

In this study, the sound absorption characteristics of a micro-periodic structure consisting of many simple resonators are investigated by numerical and theoretical analysis.

This study used numerical and theoretical analysis to investigate sound absorption characteristics of micro-periodic structures consisting of many simple resonators. The combination of different types of resonators is likewise investigated. After calculating the effective macroscopic density and sound velocity of each unit cell according to the method reported in the previous study [17], the sound absorption characteristics of quasi-single- and quasi-double-layer structures were theoretically calculated. Then, the sound absorption coefficient of 3D-printed structures using a 3D printer was measured using an impedance tube.

The basic theory of numerical and theoretical calculations is explained in Sect. 2. Section 3 describes the results of a finite element simulation and an analytical solution of the sound absorption coefficient of the samples. The experimental validation is discussed in Sect. 4, and the study is concluded in Sect. 5.

2. METHODOLOGY

The equivalent density and sound speed for each unit cell are calculated based on a microscale simulation reported by Perrot *et al.* [16] and Zieliński *et al.* [17]. This simulation performs two uncoupled analyses: scaled harmonic viscous incompressible flow and scaled harmonic thermal diffusion. Each problem is defined at the fluid domain Ω_f in the entire domain Ω of the periodic unit cell and solved for the angular frequency ω. The open porosity is given by $\phi = \Omega_f/\Omega$, and Γ_{sf} is the solid-fluid boundary inside Ω. Under a no-slip boundary condition on solid walls, a viscous flow problem developed in terms of the Ω-periodic vector field $\hat{\boldsymbol{k}}$ (normalized velocity) and the scalar field $\hat{\pi}$ (normalized pressure) is solved in the viscous incompressible flow analysis as follows:

$$\frac{j\omega}{\nu}\hat{\boldsymbol{k}} - \nabla_y^2\hat{\boldsymbol{k}} + \nabla_y\hat{\pi} = \boldsymbol{e} \quad \text{in } \Omega_f, \tag{1}$$

$$\nabla_y \cdot \hat{\boldsymbol{k}} = 0 \quad \text{in } \Omega_f, \tag{2}$$

$$\hat{\boldsymbol{k}} = 0 \quad \text{on } \Gamma_{sf} \tag{3}$$

where j, ν, and $\boldsymbol{e}$ represent the imaginary unit, the kinematic viscosity of the fluid, and the unit vector specifying the incident wave direction, respectively. $\boldsymbol{y}$ represents a spatial variable, and ∇_y denotes a gradient operator.

Alternatively, the thermal diffusion problem is solved for the normalized temperature field $\tilde{\theta}$ as follows:

$$\frac{j\omega}{\nu_{th}}\tilde{\theta} - \nabla_y^2\tilde{\theta} = 1 \quad \text{in } \Omega_f, \tag{4}$$

$$\tilde{\theta} = 0 \quad \text{on } \Gamma_{sf} \tag{5}$$

where ν_{th} is thermal diffusivity. The dynamic viscous permeability $K(\omega)$ and dynamic thermal permeability $\theta(\omega)$ can be calculated by averaging the obtained normalized velocity field $\hat{\boldsymbol{k}}$ and temperature field $\tilde{\theta}$ over the entire fluid domain Ω_f as follows:

$$K(\omega) = \phi\langle\hat{\boldsymbol{k}}(\omega)\cdot\boldsymbol{e}\rangle_f, \quad \theta(\omega) = \phi\langle\tilde{\theta}(\omega)\rangle_f \tag{6}$$

where $\langle\cdot\rangle_f$ is the average over the fluid domain Ω_f. The airflow resistivity σ can be calculated using the following equation when $\omega \to 0$:

$$\sigma = \eta/K(0) \tag{7}$$

where η represents the dynamic viscosity of air.

Then, the dynamic viscous and thermal tortuosity, $\alpha_\infty(\omega)$ and $\alpha_{th}(\omega)$, respectively, are given by

$$\alpha_\infty(\omega) = \frac{\phi\nu}{j\omega K(\omega)}, \quad \alpha_{th}(\omega) = \frac{\phi\nu_{th}}{j\omega\theta(\omega)} \tag{8}$$

These variables aid in determining the effective properties of the equivalent fluid to the porous material, including the

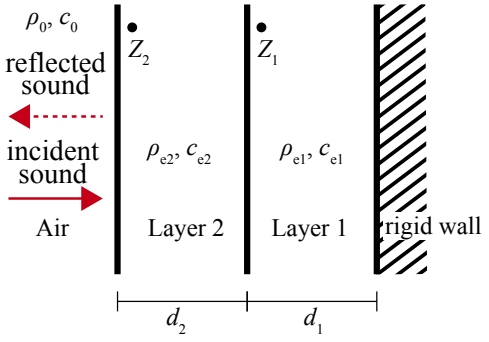

Fig. 1 Concept of the double-layer material.

effective density ρ_e and sound speed $c_e(\omega)$, as follows:

$$\rho_e(\omega) = \frac{\rho_0 \alpha_\infty(\omega)}{\phi}, \quad c_e(\omega) = \frac{c_0}{\sqrt{\alpha_\infty(\omega)\beta(\omega)}}, \tag{9}$$

$$\text{where } \beta(\omega) = \gamma - \frac{\gamma - 1}{\alpha_{th}} \tag{10}$$

where ρ_0, c_0, and γ represent the density, sound speed, and heat capacity ratio in air, respectively. After obtaining the effective density and sound speed using this microscale simulation, the surface impedance of the multilayered structure at normal incidence is calculated using the following theoretical procedure [21]. The concept of the double-layer material is shown in Fig. 1. Let $Z_{ci} = \rho_{ei} c_{ei}$, k_i, and t_i denote the characteristic effective impedance, the wavenumber, and the thickness of the i-th layers, respectively. First, the impedance of Layer 1 backed by the rigid wall is given by

$$Z_1 = -jZ_{c1} \operatorname{cotg}(k_1 t_1) \tag{11}$$

Then, the surface impedance of Layer 2 backed by Layer 1 is

$$Z_2 = Z_{c2} \frac{-jZ_1 \operatorname{cotg}(k_2 t_2) + Z_{c2}}{Z_1 - jZ_{c2} \operatorname{cotg}(k_2 t_2)} \tag{12}$$

Finally, the reflection and absorption coefficient can be estimated by applying the following equation to the surface impedance Z_i of the double-layer material obtained by the aforementioned procedure:

$$R = \frac{Z_i - \rho_0 c_0}{Z_i + \rho_0 c_0} \tag{13}$$

$$\alpha = 1 - |R|^2 \tag{14}$$

3. MICROSCALE NUMERICAL SIMULATION

3.1. Case Study

As shown in Table 1, five types of resonators were used as the unit cell. A large number of unit cells are connected to form a periodic structure, as shown in Fig. 2. The unit cell sizes are all 10 mm. The first and fourth cases are simple resonator-like structures, RES and RES2, with similar resonance frequency but different hole and cavity sizes. According to the following theoretical equation, their resonance frequencies f_c are 2,410 Hz and 2,424 Hz, respectively.

$$f_c = \frac{c_0}{2\pi} \sqrt{\frac{a}{V(l + 0.8d)}} \tag{15}$$

where V is the cavity volume, and a, l, and d are the cross-sectional area, the length, and the diameter of the hole (see Table 1). Here, the sound speed c_0 is set to 343.2 m/s.

According to Sanada and Tanaka [9], the dip in the sound absorption characteristics of a series-coupled resonator can theoretically be reduced by varying the viscous resistance of the holes. Based on their study, the three cases of RES structures with cylinder grids were newly proposed in this study to adjust the resistance of the hole as shown in Table 1. The aperture ratio was defined as the ratio of the hole area, excluding the grid part, to the incident surface area of the unit cell (10 mm × 10 mm).

This section investigates the sound absorption coefficient at normal incidence of quasi-single- and quasi-double-layer structures. The quasi-single-layer structure consists of 50-mm or 100-mm layered single unit cells, and the quasi-double-layer structure consists of two types of 50-mm layered unit cells, each for a total of 100 mm.

3.2. Calculation Settings

The microscale simulation described in Sect. 2 was implemented in the finite element analysis software (COMSOL Multiphysics® version 5.6). The validity of the calculation was confirmed by the benchmark problem [17]. The model settings are illustrated in a two-dimensional diagram using the RES-g3x3 structure as an example in Fig. 3. The spatial domain was discretized by the tetrahedral elements, and the minimum and maximum mesh sizes were 1.8e-4 mm and 1 mm, respectively. No-slip and isothermal conditions were set at solid-fluid boundaries. Periodic conditions were applied for unit cell boundaries as appropriate. The calculation assumed another zero-depth hole with the same diameter on the face opposite the hole with grids, as shown in (b) backside condition in Fig. 3. This simulation was conducted for the 1/12 octave band center frequencies, from 100 Hz to 4 kHz. Using the obtained effective properties, the absorption coefficients of the quasi-single- and quasi-double-layer samples were calculated theoretically.

3.3. Results and Discussion

3.3.1. Quasi-single-layer structure

As a prerequisite, the sound absorption coefficients for a quasi-single-layer (50 and 100 mm) of the basic unit cells

Table 1 Numerical model and geometrical parameters of unit cells. RES and RES2 denote two types of resonator-like unit cells with different hole and cavity sizes. Note that g*x* indicates the number of grids of the hole. For example, in the case of g1x1, two cylinders intersected at the center of the hole.

	RES	RES-g1x1	RES-g3x3	RES2	RES2-g3x3
Solid domain	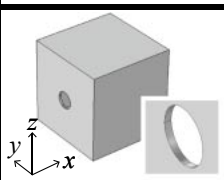	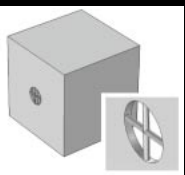	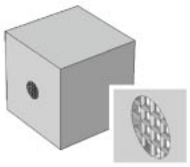	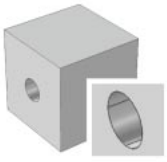	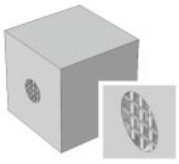
Fluid domain	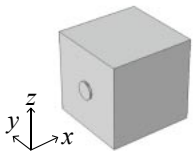				
Hole geometry [mm]		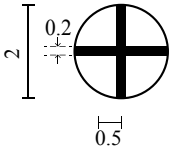	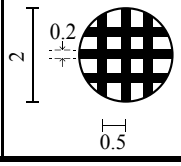	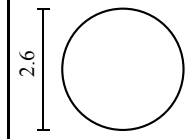	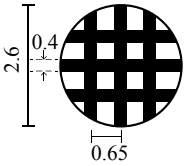
Unit cell size	(x) 10 mm × (y) 10 mm× (z) 10 mm				
Neck size	0.25 mm			1.5 mm	
Grid position (x)		0.1 mm			0.24 mm
Wall thickness	0.25 mm				
Cavity size	(x) 9.75 mm × (y) 9.5 mm× (z) 9.5 mm			(x) 8.5 mm × (y) 9.5 mm× (z) 9.5 mm	
Porosity [-]	0.8807	0.8806	0.8804	0.7751	0.7737
Aperture ratio [-]	0.031	0.024	0.013	0.053	0.011

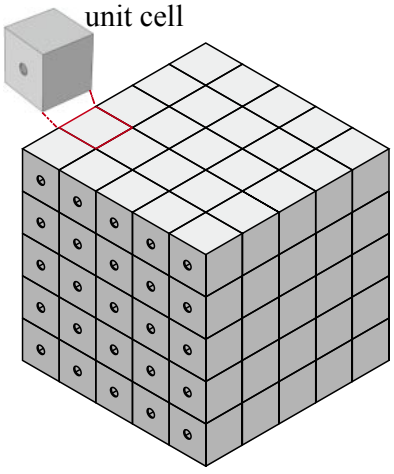

Fig. 2 Periodic structure created by resonator-like unit cells (e.g., RES).

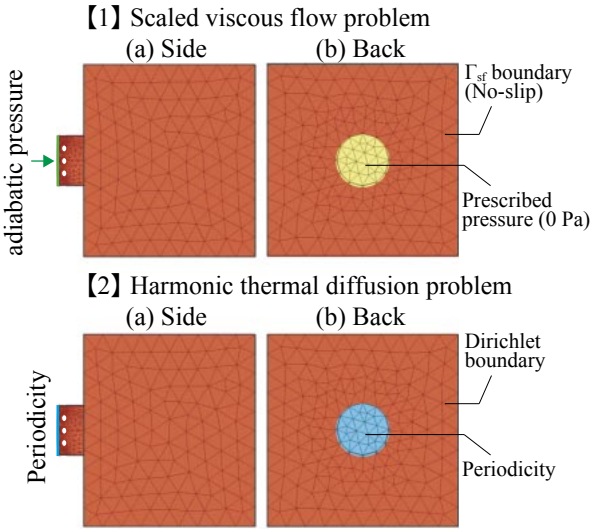

Fig. 3 Example of a microscale simulation model: (a) side and (b) backside.

are shown in Figs. 4(a) to 4(f). For comparison with the conventional specimen, the figures also show the theoretical result of a glass wool board (96 kg/m^3) with the same thickness (from now on, GW96k). This data was obtained by Miki model [22], assuming airflow resistivity of 50,000 Pa·s/m^2. Figure 5 shows the relationship between the airflow resistivity and the aperture ratio of each unit cell.

Consider the two types of resonator-like unit cells with no grids, RES and RES2. As shown in Figs. 4(a) and 4(b), the sound absorption is slightly higher for RES. However,

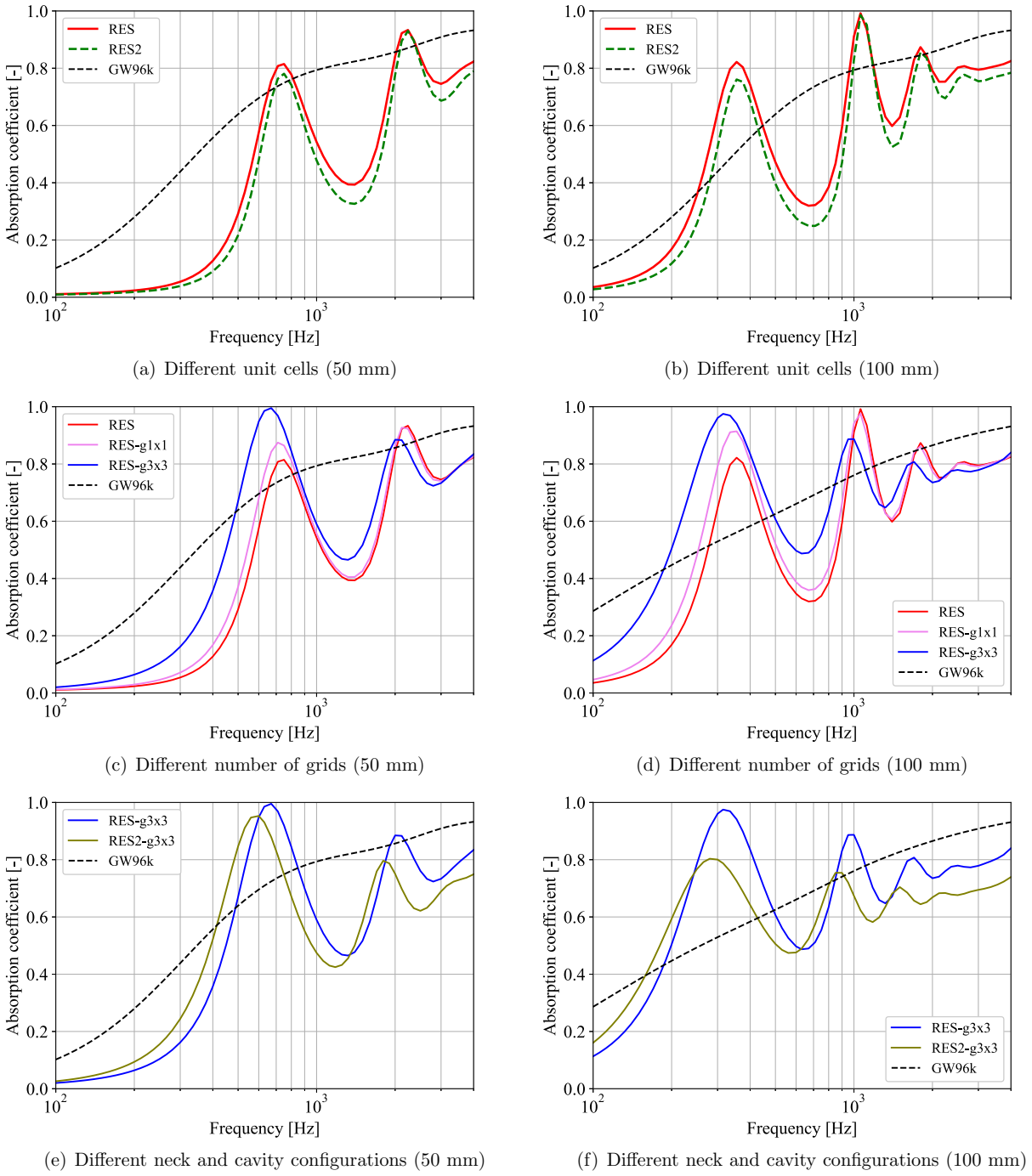

(a) Different unit cells (50 mm)

(b) Different unit cells (100 mm)

(c) Different number of grids (50 mm)

(d) Different number of grids (100 mm)

(e) Different neck and cavity configurations (50 mm)

(f) Different neck and cavity configurations (100 mm)

Fig. 4 Absorption coefficient of quasi-single-layer structures with different parameters about the cylinders.

they have nearly the same performance, despite the difference in hole and cavity sizes. There is also no significant difference in terms of the airflow resistivity shown in Fig. 5.

Next, to evaluate the effect of the vertical connection, we consider the resonance frequencies of a single resonator with same cavity size as the 100-mm-thick RES or RES2. The resonance frequency of a single resonator with same cavity sizes as 10 connected RES unit cells, i.e., with a hole of 2.6 mm in diameter and a cavity of 9.5 mm × 9.5 mm × 97.5 mm (volume excluding the hole length), is calculated to be 762 Hz. Similarly, for a single resonator with the same cavity size as 10 connected RES2, the resonance frequency is 767 Hz. The resonator peaks of the 100-mm-thick RES and RES2 are found at about 350 Hz, 1 kHz, and 1.8 kHz, with several lower and higher resonance peaks than the single resonator. This indicates that the RES and RES2 structures have the characteristics of a series-coupled resonator with multiple prominent peaks. Furthermore, their values increase with the frequency, which is not a resonator-like property, where sound absorption is significant around the resonance frequency. Because of the higher

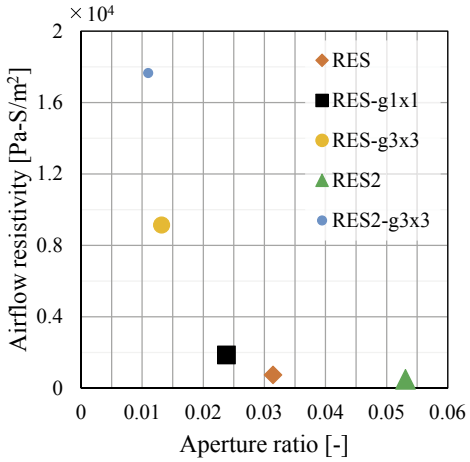

Fig. 5 Relationship between airflow resistivity and aperture ratio.

sound absorption coefficient at higher frequencies, these structures exhibit sound-absorbing properties of porous materials by arranging numerous resonators vertically and horizontally.

The results of the three types of quasi-single-layer RES and RES2 structures with grids are shown in Figs. 4(c) to 4(f). The results are used to investigate the effect of several geometric parameters on sound absorption characteristics. All types of RES structures exhibit multiple peaks and dips due to the characteristics of a series-coupled resonator in the low-frequency range, and the values are high in the higher frequency range due to porous material-like behavior.

Figures 4(c) and 4(d) show the results of two cases with the same diameter and different numbers of cylinders and the case with no grid, respectively. The increase in the viscous resistance of the holes by the number of grids leads to the smaller dips and better sound absorption characteristics below 1 kHz. For example, RES-g3x3 (100 mm) has a high sound absorption coefficient owing to the resonance around 300 Hz and stable sound absorption of 0.7–0.8 in 1–4 kHz. As shown in Fig. 5, a larger number of grids leads to greater airflow resistivity, which may contribute to the difference in sound absorption characteristics. A structure with higher airflow resistivity exhibits a stable sound absorption coefficient with small dips, whereas that with lower airflow resistivity exhibits steeper peaks. Notably, the resonance frequencies of RES-g1x1 and RES-g3x3 are slightly lower than RES due to the smaller cross-sectional area of the holes. Although inferior to the conventional glass wool GW96k in the range without resonance peaks, RES structures have significantly higher sound absorption coefficients around low and middle peak frequencies.

The results for RES-g3x3 and RES2-g3x3, which have the same number of grids, are shown in Figs. 4(e) and 4(f), respectively. The results with no grid shown in Fig. 4(b) indicate that the effect of the difference in hole and cavity size is small. However, RES-g3x3 exhibits a significantly higher sound absorption coefficient than RES2-g3x3, especially at peak frequencies, as shown in Fig. 4(f). Figure 5 shows that there is a large difference between RES-g3x3 and RES2-g3x3 in terms of the airflow resistivity, even though they have similar aperture ratios. This difference may be attributed to the geometric relationship between the hole and grid, such as the volume ratio and the grid position. The detailed investigation will be subject to future studies.

Nevertheless, the proposed structures, especially RES-g3x3 and RES2-g3x3, which consist of many resonators with grids, have both series-coupled resonator and porous material characteristics and can be excellent sound-absorbing material covering a wide range of frequencies. Note that most current 3D printers have difficulty producing delicate patterns of less than 0.4 mm in diameter. However, the accuracy of 3D printers has been improving rapidly, and soon it will be possible to produce delicate structures such as RES-g3x3.

3.3.2. Quasi-double-layer structure

To examine the sound absorption coefficient when two layers of different structures are combined, we consider the results of combining two types of resonators. RES2 and RES2-g3x3 are the resonator-like unit cells under consideration, assuming printing on a 3D printer. The legend represents "(material in Layer 1)_(material in Layer 2)" (see Fig. 1). For example, when the RES2-g3x3 is placed in Layer 1 (the back wall side) and the RES2 is in Layer 2 (incident side), this case is written as RES2-g3x3_RES2.

Figure 6 shows the results of combining RES2 with steep peaks and RES2-g3x3 with a stable and high sound absorption coefficient. RES2_RES2-g3x3 has a similar gradual peak as RES2-g3x3, and the dip is smaller than in RES2. Alternatively, RES2-g3x3_RES2 exhibits the steep

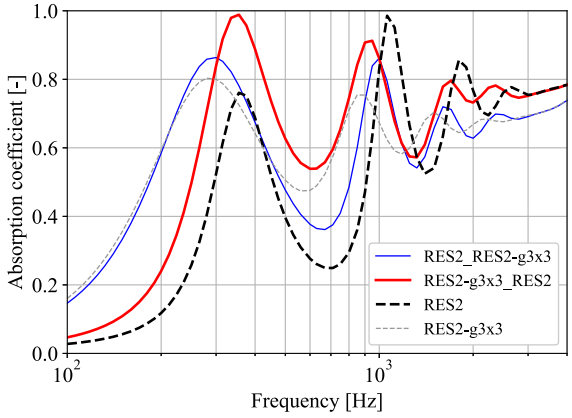

Fig. 6 Absorption coefficient of quasi-double-layer structure.

peak characteristic of RES2 to a large extent and shows a stable high sound absorption with a slight dip due to RES2-g3x3. This result shows that combining two materials results in a sound absorption characteristic that combines their properties. In particular, the influence of the material properties on the incident side (Layer 2) is significant. Therefore, combining two resonator-like structures with high and low airflow resistivity enables the realization of the stable sound absorption with a slight dip while keeping the peak somewhat large. Additionally, the large contribution of the incident side material indicates that the structure with lower airflow resistivity should be placed on the incident side to achieve higher sound absorption performance by taking advantage of both. In the high-frequency range, these combinations exhibit a similar sound absorption coefficient as that for a quasi-single-layer structure of the Layer 2 material.

These considerations indicate that the sound absorption characteristics may be controlled in various ways by combining each structure.

4. MEASUREMENT

4.1. Measurement Settings

RES2 and RES2-g3x3 were 3D-printed for the validation of calculation results in the previous section. Each structure was designed in AutoCAD (Autodesk Inc.) and output as a standard triangulated language (STL) file. Then, this model was 3D-printed using a stereolithography 3D printer XFAB2000 (DWS). During the 3D-printing process, the platform moves to the resin tank below and is filled with resin, and the laser solidifies each layer in turn. Repeating this process transforms the liquid resin into a 3D solid object. The base material is a dedicated ceramic blended resin (Therma 294). The 3D-printed samples for the large and small impedance tubes are shown in Fig. 7.

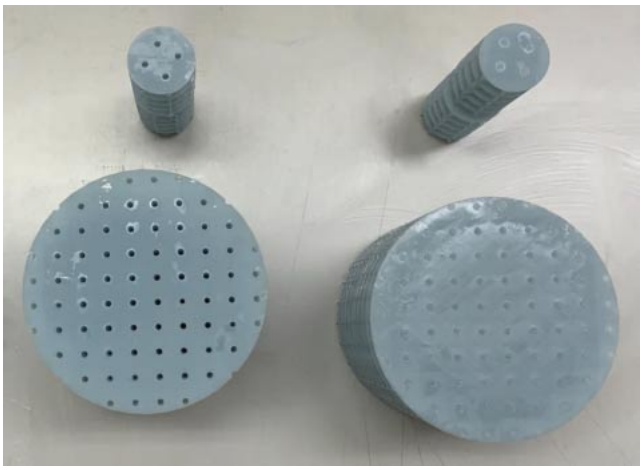

Fig. 7 3D-printed samples: RES2 (left) and RES2-g3x3 (right). Top and bottom samples are for small and large tubes, respectively.

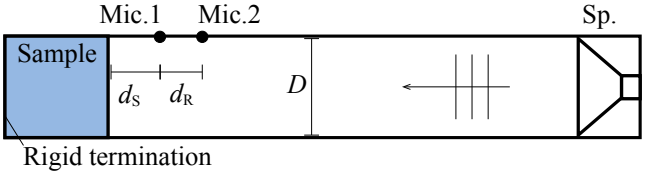

Fig. 8 Measurement setup of an impedance tube. M1 and M2 depict two microphone positions. d_S is the distance between the sample and M1, and d_R is that between the two microphones.

The sample thickness was 100 mm consisting of two 3D-printed 50-mm-thick structures.

A problem occurred when the liquid resin remained inside the structure after completing the printing process. This problem was especially noticeable with RES2-g3x3, a small aperture ratio. We left the specimens for several days to drain as much residual resin as possible to address this problem.

The sound absorption coefficients at normal incidence of the 3D-printed samples were measured using an impedance tube kit (Type 4206, Brüel and Kjær) with the large (100 mm) and small (29 mm) diameter. The measurement setup is illustrated in Fig. 8. Two 1/4 inch microphones (Type 4939, Brüel and Kjær) were placed at M1 and M2. The distances d_S and d_R for the large tube were 100 and 50 mm, and those for the small tube were 35 and 25 mm, respectively. The measurements complied with the ISO 10534-2 international standard (the transfer function method) [23], and the results were obtained using the dedicated software PULSE LabShop. The source signal was 17-seconds of white noise. The lower and upper limits of the measurement frequency were set to 100–1,600 Hz for the large tube and 200–4,000 Hz for the small tube, and the frequency resolution was 2 Hz for both.

4.2. Results and Discussion

Figure 9 shows the measurement and calculation results of quasi-single- and quasi-double-layer structures. Although the results for the large and small tubes are sometimes combined, they are presented separately to examine the differences between samples in this study. All graphs show that the trends of both calculated and experimental results are generally consistent, indicating the validity of the calculated results. However, the experimental and calculated results have several discrepancies. The results for the small tube show a larger peak dip and sometimes have different peaks in the high-frequency range compared to the calculated sound absorption coefficients. This tendency may be caused by the smaller cavity sizes of the unit cells at the periphery. Moreover, as shown in Figs. 9(b) to 9(d), the large tube results using RES2-g3x3 exhibit significant disagreement

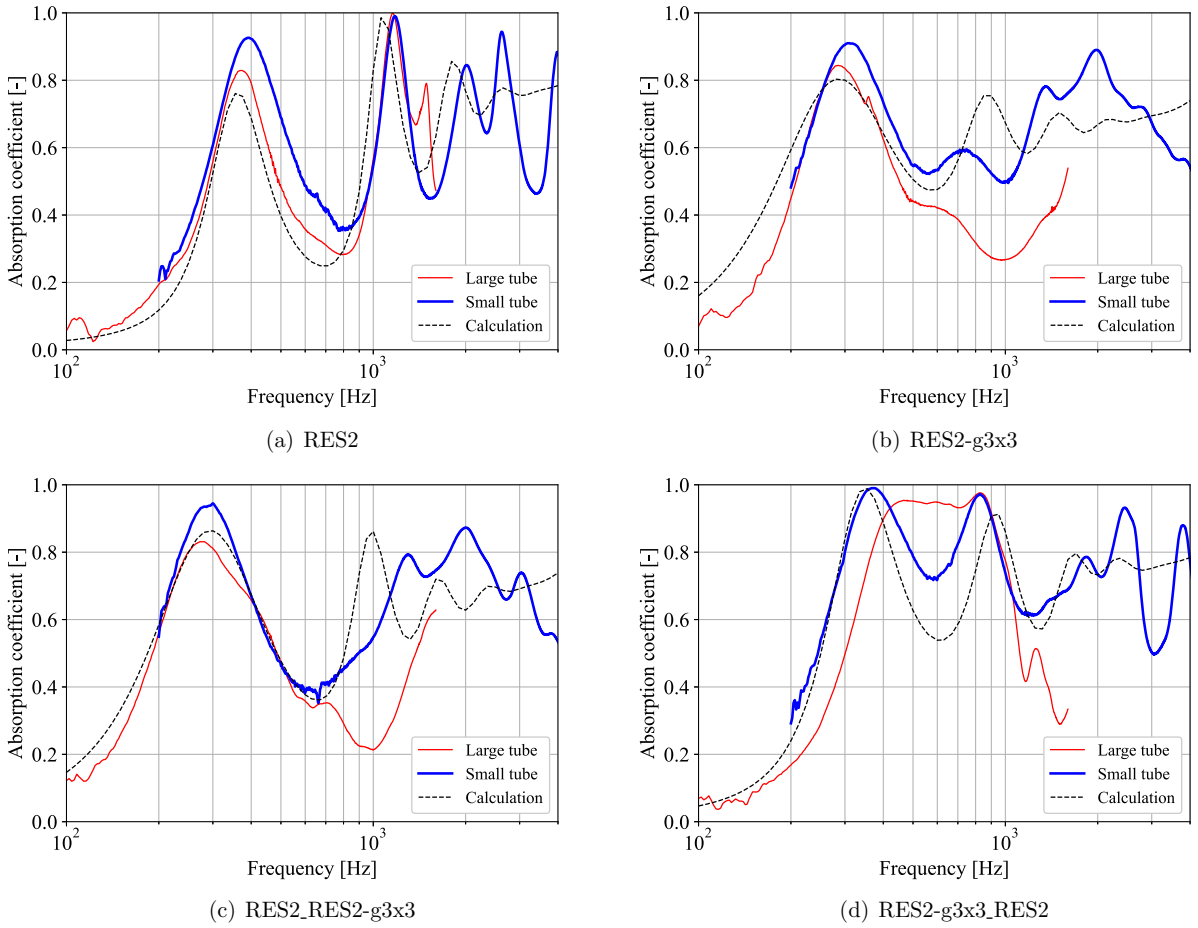

(a) RES2 (b) RES2-g3x3

(c) RES2_RES2-g3x3 (d) RES2-g3x3_RES2

Fig. 9 Measured and calculated absorption coefficients.

with the calculated data. Such discrepancy may be due to the effect of the remaining liquid resin inside the structure. Structural solutions, such as drilling lateral holes, may be considered, but this is a future issue.

Despite some discrepancies as explained above, the 3D-printed quasi-single-layer structures show both characteristics of coupled resonator and the porous material as same as the calculation results. The quasi-double-layer specimens exhibit the combined characteristics of the two structures. These findings indicate the usefulness of the 3D-printed structures as the sound-absorber.

5. CONCLUSION

Sound-absorbing materials for low- and middle-frequency ranges consisting of micro-periodic structures based on the resonator-like unit cells were investigated by numerical and theoretical procedures. The performance of the 3D-printed specimens was also measured using the impedance tube, verifying the calculation results. Based on the obtained results, the following conclusions were drawn.

The quasi-single-layer structures showed that a structure consisting of many resonators connected horizontally and vertically had both a high sound absorption coefficient at low resonance frequencies and porous material-like characteristics where the sound absorption coefficient increases with frequency. Furthermore, attaching a grid to the resonator hole enabled a high sound absorption coefficient for low and middle frequencies over a wide area. In addition, it was suggested that grid parameters such as the number and fineness might affect the airflow resistivity and the sound absorption performance.

A discussion of the quasi-double-layer structure showed that both characteristics can be added, and the way each character appears depends on how it is combined with different structures. In addition, a combination of different types of resonator-based periodic structures can be a good sound-absorber for low- and middle-frequency ranges that can be adapted to situations more flexibly. Thus, for example, it is possible to prepare units or 3D models of a specific size and design a sound absorber by combining them according to the frequency range one wants to absorb.

These findings suggest the possibility of reproducing a high degree of freedom in sound absorption performance depending on the conditions by freely combining the different structures as discussed using additive manufac-

turing. We will further analyze these sound-absorbing structures in detail, such as grid parameters, and we aim to establish an additive manufacturing design method for artificial sound-absorbing materials. It is also necessary to design structures that can appropriately handle the residual resin inside.

ACKNOWLEDGMENT

This work was supported by JSPS KAKENHI Grant Number JP20K22453. I am grateful to ENAGO, Crimson Interactive Pvt. Ltd., for carefully proofreading the manuscript.

REFERENCES

[1] K. Tatematsu, S. Hirota, H. Suzuki, M. Taniguchi, Y. Nunoi and T. Uzawa, "Influence of temperature and moisture on aging of glass wool," *J. Environ. Eng.*, **79**, 753–762 (2014) (in Japanese).

[2] D. Y. Maa, "Theory and design of microperforated panel sound-absorbing constructions," *Sci. Sin.*, **17**, 55–71 (1975).

[3] D. Y. Maa, "Microperforated panel wideband absorber," *Noise Control Eng. J.*, **29**, 77–84 (1987).

[4] K. Sakagami, M. Morimoto and W. Koike, "A numerical study of double-leaf microperforated panel absorbers," *Appl. Acoust.*, **67**, 609–619 (2006).

[5] H. V. Fuchs and X. Zha, "Acrylic-glass sound absorbers in the plenum of the deutscher bundestag," *Appl. Acoust.*, **51**, 211–217 (1997).

[6] H. Drotleff and X. Zhou, "Attractive room acoustic design for multi-purpose halls," *Acta Acust. united Ac.*, **87**, 500–504 (2001).

[7] K. Hoshi, T. Hanyu, T. Okuzono, K. Sakagami, M. Yairi, S. Harada, S. Takahashi and Y. Ueda, "Implementation experiment of a honeycomb-backed mpp sound absorber in a meeting room," *Appl. Acoust.*, **157**, 107000 (2020).

[8] K. Sakagami, Y. Fukutani, M. Yairi and M. Morimoto, "A theoretical study on the effect of a permeable membrane in the air cavity of a double-leaf microperforated panel space sound absorber," *Appl. Acoust.*, **79**, 104–109 (2014).

[9] A. Sanada and N. Tanaka, "Investigation of characteristics of sound absorbers with series-coupled helmholtz resonators," *J. Acoust. Soc. Jpn.* (*J*), **62**, 759–766 (2006) (in Japanese).

[10] A. Sanada and N. Tanaka, "Extension of the frequency range of resonant sound absorbers using two-degree-of-freedom helmholtz-based resonators with a flexible panel," *Appl. Acoust.*, **74**, 509–516 (2013).

[11] R. Al Jahdali and Y. Wu, "Coupled resonators for sound trapping and absorption," *Sci. Rep.*, **8**, 13855 (2018).

[12] Y. Tang, S. Ren, H. Meng, F. Xin, L. Huang, T. Chen, C. Zhang and T. Lu, "Hybrid acoustic metamaterial as super absorber for broadband low-frequency sound," *Sci. Rep.*, **7**, 43340 (2017).

[13] M. Yang, S. Chen, C. Fu and P. Sheng, "Optimal sound absorbing structures," *Proc. Meet. Acoust.*, **32**, 045018 (2017).

[14] S. Deshmukh, H. Ronge and S. Ramamoorthy, "Design of periodic foam structures for acoustic applications: Concept, parametric study and experimental validation," *Mater. Des.*, **175**, 107830 (2019).

[15] S. Gasser, F. Paun and Y. Bréchet, "Absorptive properties of rigid porous media: Application to face centered cubic sphere packing," *J. Acoust. Soc. Am.*, **117**, 2090–2099 (2005).

[16] C. Perrot, F. Chevillotte and R. Panneton, "Bottom-up approach for microstructure optimization of sound absorbing materials," *J. Acoust. Soc. Am.*, **124**, 940–948 (2008).

[17] T. G. Zieliński, R. Venegas, C. Perrot, M. Červenka, F. Chevillotte and K. Attenborough, "Benchmarks for microstructure-based modelling of sound absorbing rigid-frame porous media," *J. Sound Vib.*, **483**, 115441 (2020).

[18] K. C. Opiela and T. G. Zieliński, "Microstructural design, manufacturing and dual-scale modelling of an adaptable porous composite sound absorber," *Composites Part B: Eng.*, **187**, 107833 (2020).

[19] T. Yamamoto, S. Maruyama, K. Terada, K. Izui and S. Nishiwaki, "A generalized macroscopic model for sound-absorbing poroelastic media using the homogenization method," *Comput. Methods Appl. Mech. Eng.*, **200**, 251–264 (2011).

[20] T. G. Zieliński, K. C. Opiela, P. Pawłwski, N. Dauchez, T. Boutin, J. Kennedy, D. Trimble, H. Rice, B. Van Damme, G. Hannema, R. Wróbel, S. Kim, S. Ghaffari Mosanenzadeh, N. X. Fang, J. Yang, B. Briere de La Hosseraye, M. C. J. Hornikx, E. Salze, M. A. Galland, R. Boonen, A. Carvalho de Sousa, E. Deckers, M. Gaborit and J. P. Groby, "Reproducibility of sound-absorbing periodic porous materials using additive manufacturing technologies: Round robin study," *Addit. Manuf.*, **36**, 101564 (2020).

[21] J. F. Allard and N. Atalla, *Propagation of Sound in Porous Media: Modelling Sound Absorbing Materials*, 2nd ed. (John Wiley & Sons, Chichester, 2009), Chap. 2, pp. 15–27.

[22] Y. Miki, "Acoustical properties of porous materials — modifications of delany-bazley models —," *J. Acoust. Soc. Jpn.* (*E*), **11**, 19–24 (1990).

[23] ISO 10534-2: 1998 acoustics — determination of sound absorption coefficient and impedance tubes part 2: Transfer function method. Standard (1998).